AN4402
Application note

Multichannel drivers driving inductive loads with L99MC6 and L9733

Introduction

The L99MC6 and the L9733 are respectively hexa and octal multi-channel drivers capable of driving various types of loads: resistive, inductive, capacitive loads and LEDs. They integrate an SPI interface for a high level of configurability, offering detailed device diagnostics and protection features such as overtemperature, overcurrent detection, in order to support robust automotive designs.

The output stages of these flexible devices consist of n-channel MOSFETs. They both have an internal charge pump which allows all the outputs of the L9733 and three outputs of the L99MC6 (outputs 1, 2, 3) to control loads either in high-side or in low-side configuration without additional components. The L99MC6 outputs 4, 5 and 6 are fixed low-side drivers.

Figure 1. Block diagrams on the L99MC6 and L9733

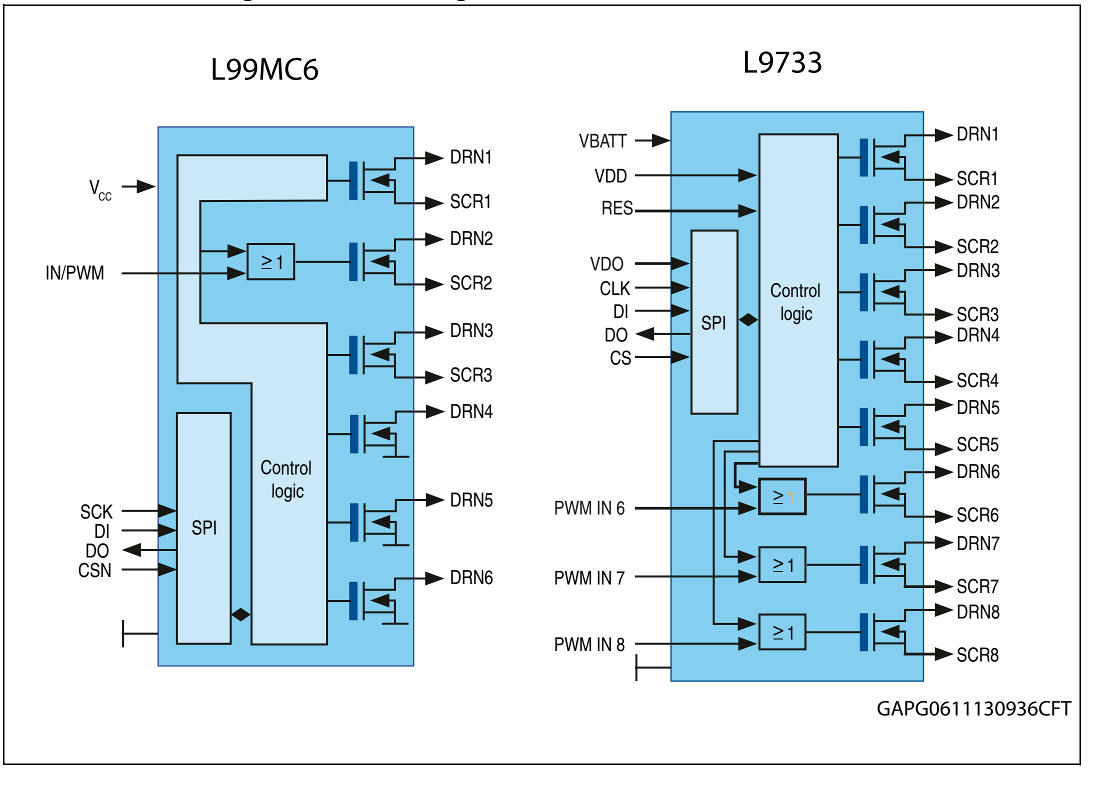

Contents

List of tables

List of figures

1 Description

This document describes the protection features implemented in the L99MC6 and L9733 to control inductive loads. It provides calculations of the energy dissipated in the output MOSFETs of these devices during the switch-off phase of this type of loads in different configurations:

- The outputs are configured either as low-side or high-side drivers
- With and without parallel resistor to the inductive load

Although the examples are applied to the L99MC6, general results are also applicable to devices integrating the same type of active clamping protections.

Finally, the developers will find a guideline to verify if the outputs of these devices are compatible with their load specifications and application conditions.

2 Active clamp of the L99MC6 and L9733

By nature, an inductive load such as a relay coil develops a voltage across its terminals in order to resist the current variations passing through it. According to Lenz's law, the voltage across the inductor is proportional to its inductance and to the rate of change of the current: $V_L = L\ di_L / dt$. This voltage can reach very high values when the current is abruptly turned off.

Opening mechanically a circuit with an energized inductor without any protection will result in a high voltage surge across the load of possibly several hundreds of volts, which can cause an electrical arc.

During the turn-off phase of a MOSFET driving an inductive load the voltage across the drain and the source of the MOSFET (V_{DS}) will increase until the MOSFET breakdown voltage is reached. It is the so-called avalanche effect. Operating in avalanche can have a negative impact on the lifetime of standard MOSFETs.

The output stages of the L99MC6 and of the L9733 consist of protected n-channel MOSFETs which can be driven either in low-side or high-side configuration. In order to avoid avalanche conditions during the switch-off of an inductive load, the L99MC6 and the L9733 integrate a so-called active clamp, which limits V_{DS} below the MOSFETs' breakdown (*Figure 2*). Indeed, during the turn-off of inductive loads, the output MOSFET is driven in linear (and high dissipation) mode. This results in a higher control capability of this type of loads without additional devices.

Figure 2. Low-side and high-side configured output driving inductive loads

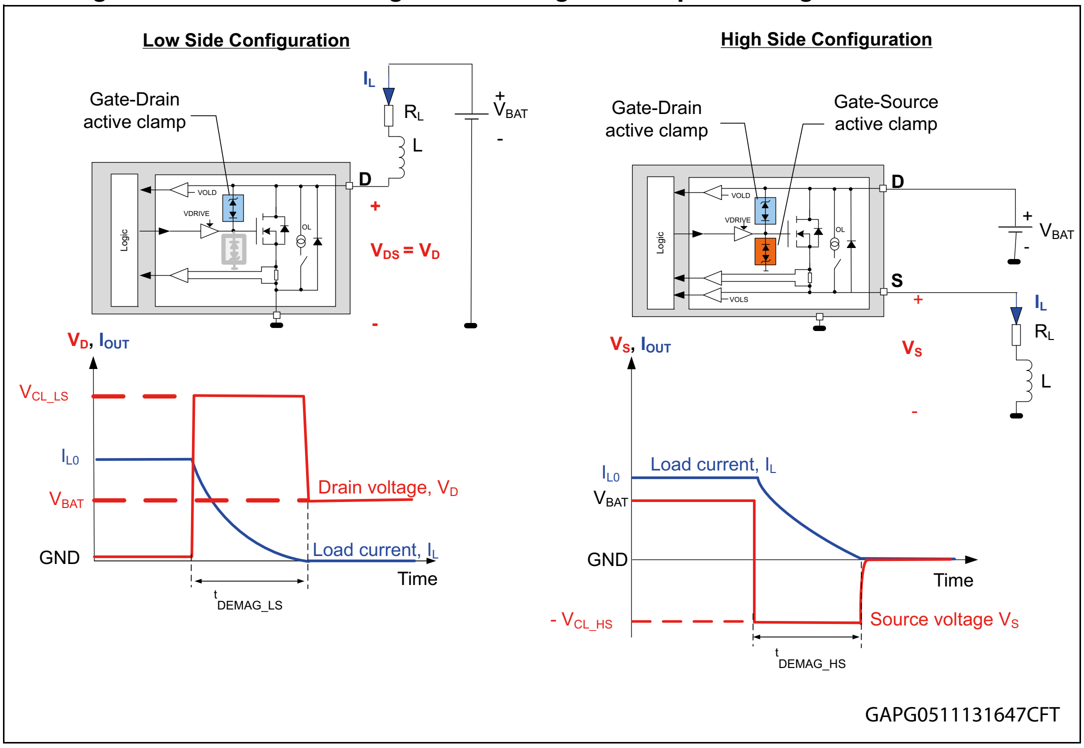

2.1 Low-side configured outputs

Right after the turn-off of a low-side switch, the inductor current decreases, and V_L goes negative with the sign convention (*Figure 3*). Consequently, the MOSFET drain-source voltage V_{DS} increases until V_{DS} reaches $V_{ZENER\_LS} + V_F + V_{GS\_TH} = V_{CL\_LS}$. At this moment the MOSFET is turned back on in linear mode.

The control loop consisting of a zener between the MOSFET gate and drain (*Figure 3*) is called the gate-drain clamp in the rest of the document. This circuits maintains V_{DS} (=V_D, since the source is connected to GND in this case) to V_{CL_LS} until the energy stored in the inductor is completely dissipated (waveform on *Figure 2*). V_{CL_LS} has been chosen below the MOSFET breakdown in order to avoid the avalanche conditions. This protection reduces the stress applied to the MOSFET.

Figure 3. Low-side of a L99MC6 during the turn-off phase

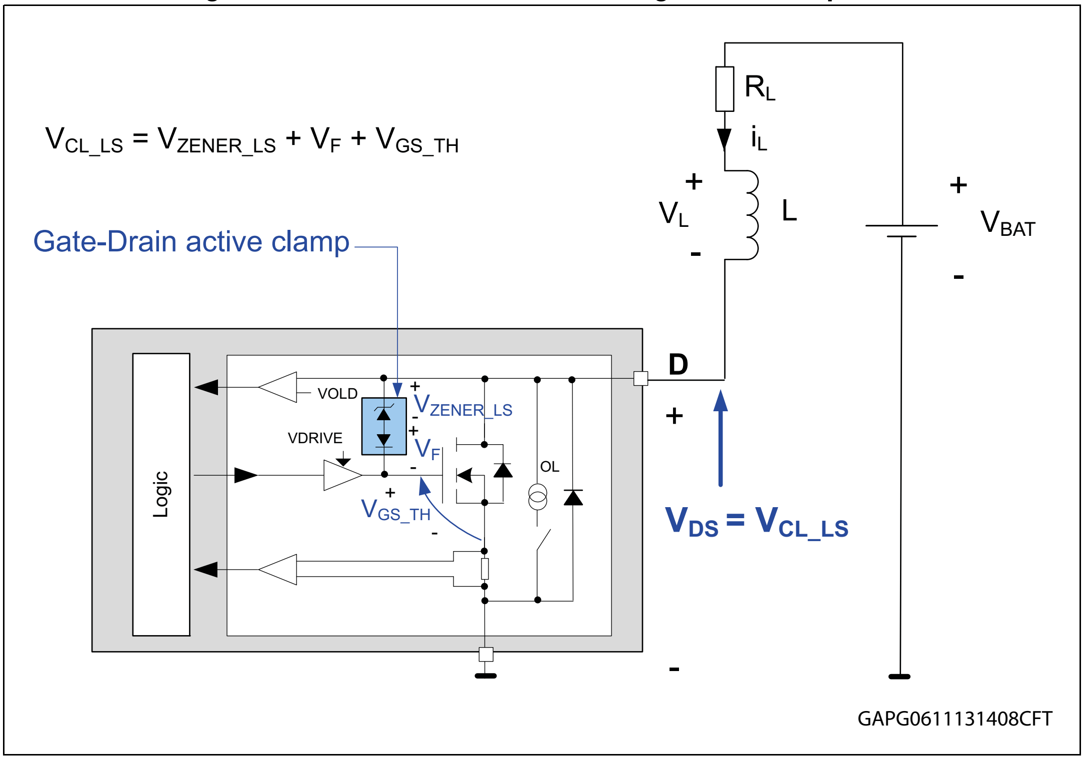

2.2 High-side configured outputs

For a high-side configured output, either the gate-drain clamp or the gate-source clamp is activated (*Figure 7* and *Figure 8*), depending on the conditions.

We can distinguish two cases:

- Case 1: $V_{BAT} < V_{CL\_LS} - V_{CL\_HS}$
- Case 2: $V_{BAT} > V_{CL\_LS} - V_{CL\_HS}$

2.2.1 Case 1: $V_{BAT} \leq V_{CL\_LS} - V_{CL\_HS}$

During turn-off, the evolution of the voltage across the inductor causes V_S to go negative (*Figure 2*) and the gate-source clamp (*Figure 3*) is activated when $V_S = -V_{CL\_HS}$.

Note: In this document V_{CL_HS} is considered positive.

V_S is maintained at $-V_{CL\_HS}$. Therefore $V_{DS} = V_{BAT} + V_{CL\_HS} < V_{CL\_LS}$ and the gate-drain clamp is not activated.

Figure 4. L99MC6 high-side during the turn-off, $V_{BAT} < V_{CL\_LS} - V_{CL\_HS}$

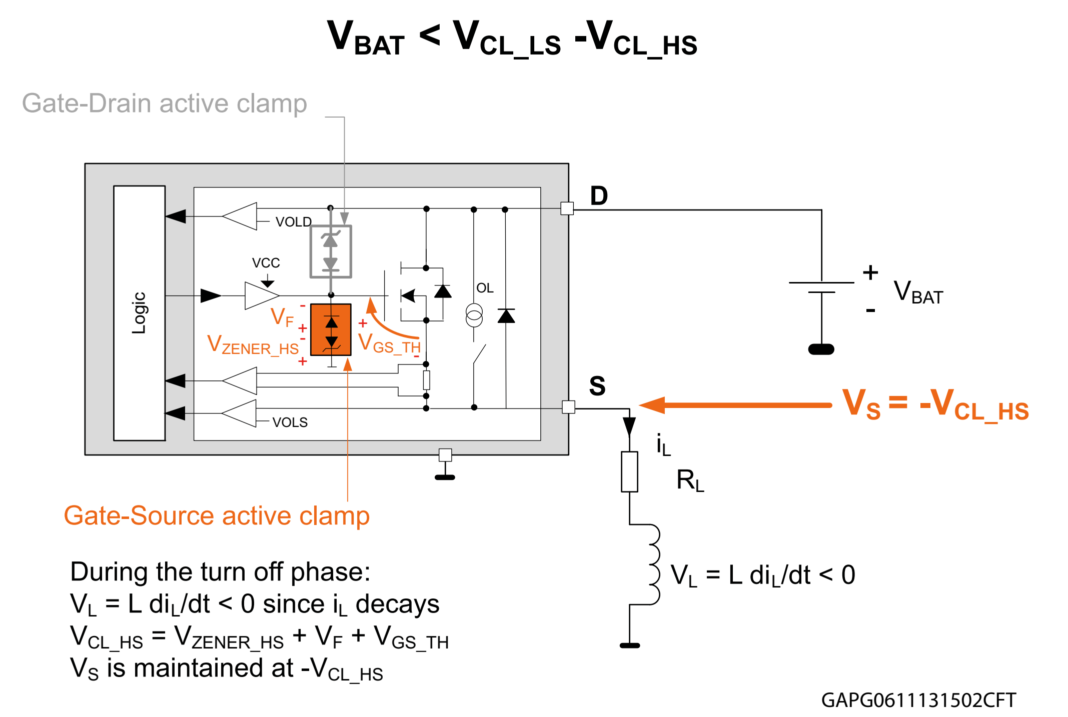

Case 1 corresponds to a demagnetization of the inductive load at typically $V_{BAT} \leq 16$ V for the L99MC6 and at $V_{BAT} \leq 36$ V for the L9733. It is applicable to the nominal battery voltage for automotive applications (13.5 V).

Note: The gate-source clamp only maintains V_S to $-V_{CL\_HS}$. i_L is still supplied by the battery and not by the gate-source clamp.

Table 1. Specification of clamping voltages - L99MC6 and L9733

	L99MC6	L9733
Typ. V_{CL_LS}	35 V Datasheet parameter: V_{DRN_CL1-6}	55 V Datasheet parameter: DRN1-8CL
Typ V_{CL_HS}	19 V Datasheet parameter: $\lvert V_{SRC\_CL1-3} \rvert$	19 V Datasheet parameter: |SRC_1-8CL|
V_{BAT} limit for case1 / case2	16 V	36 V

2.2.2 Case 2: $V_{BAT} \geq V_{CL\_LS} - V_{CL\_HS}$

At the turn-off, the evolution of the voltage across the inductor causes an increase of V_{DS} until $V_{DS} = V_{CL\_LS}$. Then, the gate-drain clamp is activated (see *Figure 5*), like for a low-side switch. V_{DS} is maintained at $V_{CL\_LS} = V_{ZENER\_HS} + V_F + V_{GS\_TH}$.

Since $V_S = V_{BAT} - V_{CL\_LS} > - V_{CL\_HS}$, this prevents the activation of the gate-source clamp.

Figure 5. L99MC6 high-side during the turn-off, $V_{BAT} > V_{CL\_LS} - V_{CL\_HS}$

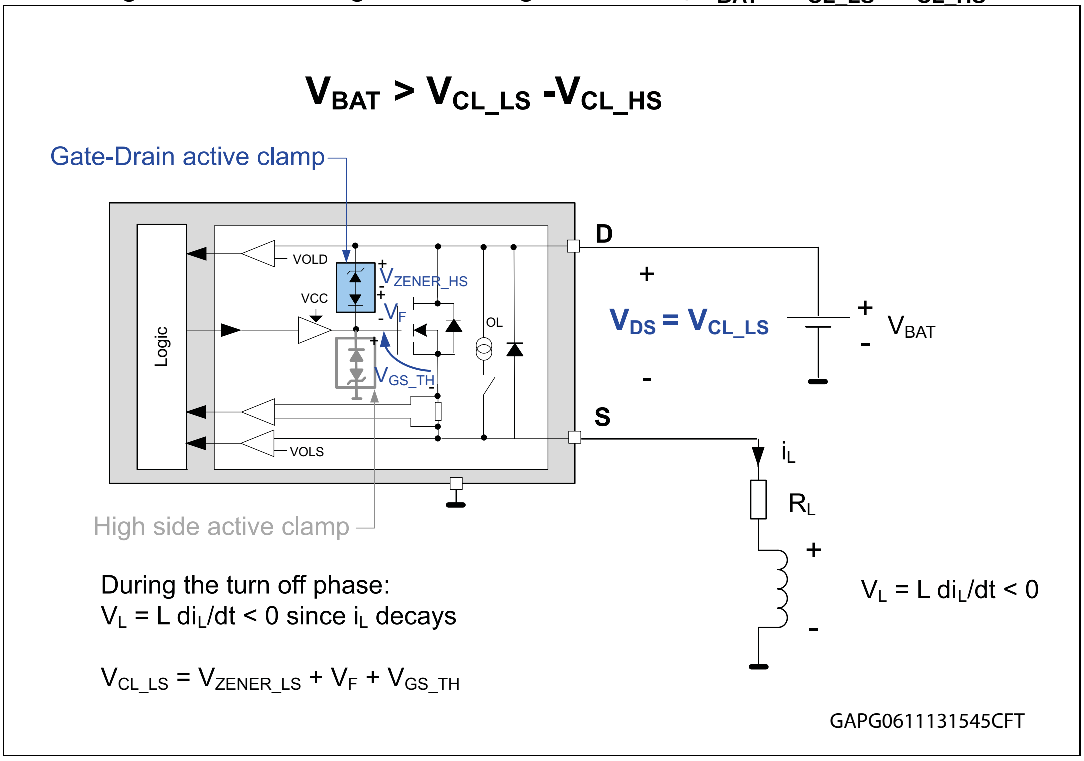

Case 2 corresponds to a demagnetization of the inductive load for $V_{BAT} \geq 16$ V for the L99MC6 and for $V_{BAT} \geq 36$ V for the L9733.

3 Demagnetization energy

In this section, we propose to calculate the energy dissipated in the output MOSFETs of the L99MC6 and L9733 during the switch-off of an inductive load.

We will distinguish the following conditions:

- the output is configured either as high-side or low-side driver
- with or without resistor placed in parallel (note R_P) to the inductive load

R_P is often placed in parallel to the relay coil in automotive applications in order to attenuate the voltage surge caused by the coil when the circuit is opened (*Figure 6*).

Figure 6. Relay with spike protection resistor in parallel to the coil

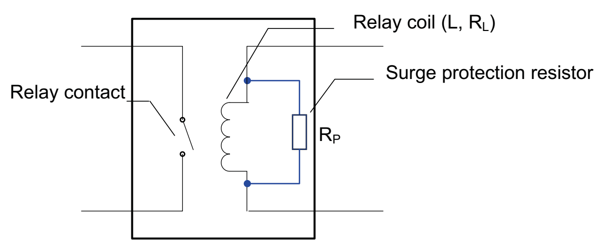

In order to determine E_{DEMAG}, we will take a deeper look at the evolution of the current flowing through the inductive load (noted i_L) and R_P (noted i_P), between the MOSFET turn-off and i_L reaching zero.

We consider:

- the time origin as the moment when the MOSFET is switched off
- the current through the inductor at t = 0 as $I_{L0} = i_L(t = 0)$
- the demagnetization time, noted t_{DEMAG}, as the time required for i_L to reach zero
- the energy dissipated in the MOSFET during the switch-off phase is noted E_{DEMAG}

3.1 Low-side configured output

Figure 7 represents the equivalent electrical diagram during the turn-off phase of a low-side configured output which drives an inductive load with parallel resistor.

Figure 7. Equivalent electrical diagram during the turn-off phase of an inductive load with parallel resistor, driven by a low-side configured output.

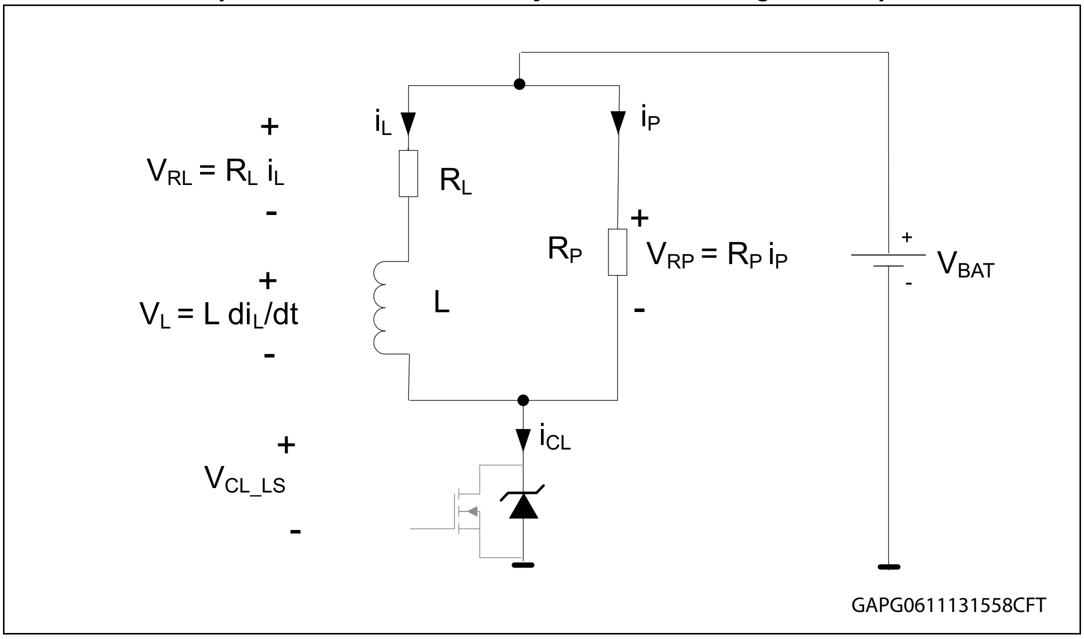

V_L is negative during the turn-off phase according to the used sign convention, since $di_L/dt < 0$.

3.2 Calculation of the demagnetization energy

Right after the turn-off, assuming that the active clamp is activated ($i_{CL} > 0$):

Equation 1

$$V_{BAT} = R_L i_L + L\frac{di_L}{dt} + V_{CL\_LS}$$

Equation 2

$$\frac{di_L}{dt} + \frac{i_L}{\tau} = \frac{V_{BAT} - V_{CL\_LS}}{\tau R_L}$$

with

$$\tau = \frac{L}{R_L}$$

Taking the time origin as the moment when the output is turned off, this differential equation (*Equation 2*) accepts the following general solutions (for $t \geq 0$):

Equation 3

$$i_L(t) = Ae^{-\frac{t}{\tau}} + \frac{V_{BAT} - V_{CL\_LS}}{R_L}$$

Where A is a constant which is determined by the boundary condition:

Equation 4

$$i_L(t = 0) = A + \frac{V_{BAT} - V_{CL\_LS}}{R_L} = I_{L0} = \frac{V_{BAT}}{R_L}$$

Substituting A with its expression in *Equation 3* gives:

Equation 5

$$i_L(t) = \frac{V_{CL\_LS}}{R_L}e^{-\frac{t}{\tau}} - \frac{V_{CL\_LS} - V_{BAT}}{R_L} \text{ (for } t \geq 0)$$

Considering that:

Equation 6

$$R_p i_p = V_{BAT} - V_{CL\_LS}$$

Equation 7

$$i_{CL}(t) = i_p(t) + i_L(t)$$

Combining *Equation 5*, *Equation 6* and *Equation 7*:

Equation 8

$$i_{CL}(t) = \frac{V_{CL\_LS}}{R_L}e^{-\frac{t}{\tau}} - \frac{V_{CL\_LS} - V_{BAT}}{R_L // R_p}$$

$R_L // R_P$ is the equivalent resistance of R_L in parallel with R_P:

Equation 9

$$R_L // R_p = \frac{1}{\frac{1}{R_L} + \frac{1}{R_p}} = \frac{R_L R_p}{R_L + R_p}$$

Equation 8 is valid if $i_{CL}(t) \geq 0$ otherwise the active clamp is not triggered. In particular at $t = 0$, $i_{CL}(t = 0) \geq 0$ is equivalent to:

Equation 10

$$R_p > \frac{V_{CL\_LS} - V_{BAT}}{V_{BAT}} R_L$$

If R_P does not satisfy this condition, the energy stored in the inductance would be dissipated only in R_L and R_P and no additional energy is dissipated in the output MOSFET.

In general, R_P is high-ohmic enough to satisfy this condition. A low-ohmic value of R_P would result in significant power losses during the activation of the relay. Moreover, this would lead to a much longer demagnetization time and possibly decreases the reliability of some loads such as relays.

Equation 8 is valid until $t = t_{DEMAG\_LS}$, where t_{DEMAG_LS} is defined by $i_{CL}(t_{DEMAG\_LS}) = 0$:

Equation 11

$$t_{DEMAG\_LS} = \frac{L}{R_L} \ln\left(\frac{V_{CL\_LS}}{V_{CL\_LS} - V_{BAT}} \frac{R_L // R_p}{R_L}\right)$$

The energy which is dissipated in the low-side driver during the turn-off phase is equal to the integration of the dissipated power $V_{CL\_LS}\, i_{CL}(t)$ from $t = 0$ to $t = t_{DEMAG}$. Using the expression of $i_{CL}(t)$ given by *Equation 8*, we obtain:

Equation 12

$$E_{DEMAG\_LS} = \int_{t=0}^{t=t_{DEMAG\_LS}} V_{CL\_LS}\left(\frac{V_{CL\_LS}}{R_L} e^{-\frac{t}{\tau}} - \frac{V_{CL\_LS} - V_{BAT}}{R_L // R_p}\right) dt$$

Finally, the demagnetization energy dissipated in the low-side driver with a parallel resistor to the inductor is:

Equation 13

$$E_{DEMAG\_LS} = V_{CL\_LS}\left(\frac{\tau}{R_L} V_{CL\_LS} - \frac{\tau}{R_L // R_p}(V_{CL\_LS} - V_{BAT})\left(1 + \ln\left(\frac{R_p}{R_L + R_p} \cdot \frac{V_{CL\_LS}}{V_{CL\_LS} - V_{BAT}}\right)\right)\right)$$

If no parallel resistor to the inductive load is present, it is possible to derive the demagnetization time and energy directly from *Figure 8*. Another possibility is to determine t_{DEMAG_LS} and E_{DEMAG_LS} in this condition from *Equation 11* and *Equation 13*, when R_P tends to $+\infty$ (and $R_L // R_P$ tends to R_L).

Figure 8. Equivalent electrical diagram of the turn-off phase of an inductive load driven by a low-side configured output, without parallel resistor to the load

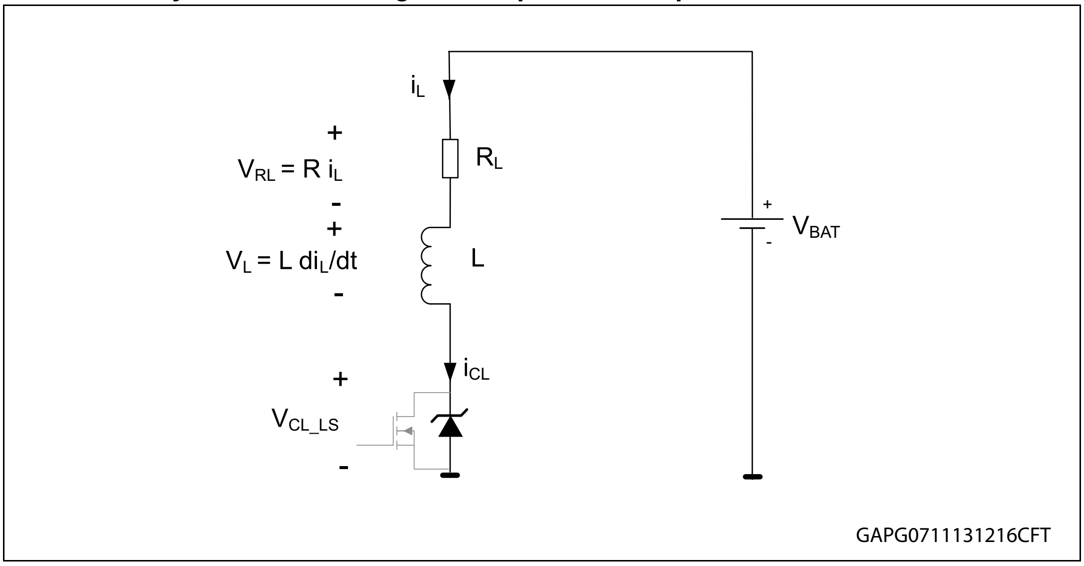

V_L is negative during the turn-off phase according to the used sign convention, since $di_L/dt < 0$.

Equation 14

$$\lim_{R_P \to +\infty} E_{DEMAG\_LS} = \frac{L}{R_L} V_{CL\_LS}\left(I_{L0} - \frac{V_{CL\_LS} - V_{BAT}}{R_L} \ln\left(\frac{V_{CL\_LS}}{V_{CL\_LS} - V_{BAT}}\right)\right)$$

Equation 15

$$\lim_{R_P \to +\infty} t_{DEMAG\_LS} = \frac{L}{R_L} \ln\left(\frac{V_{CL\_LS}}{V_{CL\_LS} - V_{BAT}}\right)$$

The theoretical case where $R_L = 0\Omega$ is considered by using $V_{BAT} = R_L I_{L0}$ for $R_L > 0$:

Equation 16

$$\ln\left(\frac{V_{CL\_LS}}{V_{CL\_LS} - V_{BAT}}\right) = \ln\left(\frac{V_{CL\_LS} - V_{BAT} + R_L I_{L0}}{V_{CL\_LS} - V_{BAT}}\right) = \ln\left(1 + \frac{R_L I_{L0}}{V_{CL\_LS} - V_{BAT}}\right)$$

Using the Maclaurin development of order 2 of $\ln(1 + x) = x - \frac{x^2}{2} + 0(x^2)$ for x in the vicinity of 0 with $x = \frac{R_L I_{L0}}{V_{CL\_LS} - V_{BAT}}$, we obtain:

Equation 17

$$\lim_{\substack{R_P \to +\infty \\ R_L \to 0}} E_{DEMAG\_LS} = \frac{1}{2} L I_{L0}^2 \left(\frac{V_{CL\_LS}}{V_{CL\_LS} - V_{BAT}} \right)$$

Equation 18

$$\lim_{\substack{R_P \to +\infty \\ R_L \to 0}} t_{DEMAG\_LS} = \frac{L I_{L0}}{V_{CL\_LS} - V_{BAT}}$$

3.2.1 Summary of the demagnetization energy – low-side

Table 2. E_{DEMAG_LS}

Conditions	Demagnetization energy in a low-side driver: E_{DEMAG_LS}
With parallel resistor to the inductive load $R_L > 0\ \Omega$	**Equation 19** $$V_{CL\_LS}\left(\frac{\tau}{R_L} V_{CL\_LS} - \frac{\tau}{R_L // R_p}(V_{CL\_LS} - V_{BAT})\left(1 + \ln\left(\frac{R_p}{R_L + R_p} \cdot \frac{V_{CL\_LS}}{V_{CL\_LS} - V_{BAT}}\right)\right)\right)$$ with $\tau = \frac{L}{R_L}$, valid if $R_p > \frac{V_{CL\_LS} - V_{BAT}}{V_{BAT}} R_L$
Without parallel resistor to the inductance $R_L > 0\ \Omega$	**Equation 20** $$\frac{L}{R_L} V_{CL\_LS}\left(I_{L0} - \frac{V_{CL\_LS} - V_{BAT}}{R_L} \ln\left(\frac{V_{CL\_LS}}{V_{CL\_LS} - V_{BAT}}\right)\right)$$ with $I_{L0} = \frac{V_{BAT}}{R_L}$
Without parallel resistor to the inductance $R_L = 0\ \Omega$	**Equation 21** $$\frac{1}{2} L I_{L0}^2 \left(\frac{V_{CL\_LS}}{V_{CL\_LS} - V_{BAT}}\right)$$ with $I_{L0} = \frac{V_{BAT}}{R_L}$

3.2.2 Calculation example

An output of the L99MC6 is configured as low-side driver and it controls an inductive load in the following conditions:

Table 3. Example of application parameters

Parameter	Value
V_{BAT}	13V
L	512mH
R_L	46Ω
R_P	200Ω - 10kΩ and no R_P ($R_P \rightarrow +\infty$)
V_{CL_LS}	35V (typical value of the L99MC6)

We verify that the condition on R_P (*Equation 10*) is satisfied: R_P must be higher than 79 Ω. Using the formulas of *Table 2*, we have:

Table 4. Energy parameters vs R_P values

R_P [Ω]	t_{DEMAG_LS} [ms]	E_{DEMAG_LS} [mJ]	E_{DEMAG_LS} decrease due to R_P [mJ]
200	2.9	8.3	15.3
300	3.6	12.4	11.2
400	4.0	14.8	8.8
600	4.3	17.5	6.1
1k	4.7	19.8	3.8
10k	5.1	23.2	0.4
No R_P ($R_P \rightarrow +\infty$)	5.2	23.6	—

Figure 9. E_{DEMAG_LS} vs R_P

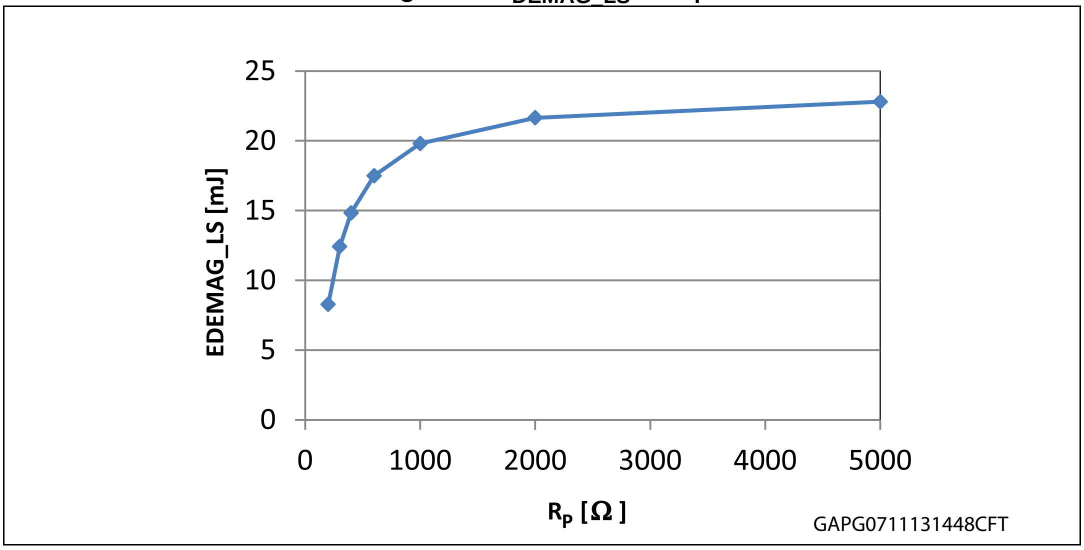

R_P dissipates a part of the energy stored in the inductor. As R_P decreases, i_P increases and the amount of energy transferred from the inductor to R_P increases as well.

Moreover, the demagnetization time decreases when R_P decreases, therefore the battery supplies less energy during the demagnetization phase.

$$t_{DEMAG\_LS} = \frac{L}{R_L} \ln\left(\frac{V_{CL\_LS}}{V_{CL\_LS} - V_{BAT}} \frac{R_L // R_p}{R_L}\right) = \frac{L}{R_L}\left(\ln\left(\frac{V_{CL\_LS}}{V_{CL\_LS} - V_{BAT}}\right) + \ln\left(\frac{R_L // R_p}{R_L}\right)\right)$$

$\ln\left(\frac{R_L // R_p}{R_L}\right)$ is negative since $R_L // R_P < R_L$. This term further decreases when R_P decreases. This explains the decrease of E_{DEMAG}, when R_P decreases.

The drawback of a low value of R_P is the fact that the power losses in R_P, when the inductive load is on, are higher as the R_P value is lower.

3.3 High-side configured outputs

3.3.1 Demagnetization energy with $V_{BAT} < V_{CL\_LS} - V_{CL\_HS}$

By similarity between the circuits displayed in *Figure 7* and *Figure 10*, we have the following equivalence between low-side and high-side configured outputs when $V_{BAT} < V_{CL\_LS} - V_{CL\_HS}$:

Low-side: $V_{CL\_LS} \leftrightarrow$ High-side: $V_{BAT} + V_{CL\_HS}$

Table 5. Analogies between the equations for a low-side and a high-side

	Low-side	High-side, $V_{BAT} < V_{CL\_LS} - V_{CL\_HS}$
V_{DS}	V_{CL_LS}	$V_{BAT} + V_{CL\_HS}$
Voltage drop across the load	V_{BAT} - V_{CL_LS}	-V_{CL_HS}
$i_L(t)$	$\frac{di_L}{dt} + \frac{i_L}{\tau} = \frac{V_{BAT} - V_{CL\_LS}}{\tau R_L}$ with $\tau = \frac{L}{R_L}$ and $I_L(t = 0) = I_{L0} = \frac{V_{BAT}}{R_L}$	$\frac{di_L}{dt} + \frac{i_L}{\tau} = -\frac{V_{CL\_HS}}{\tau R_L}$ with $\tau = \frac{L}{R_L}$ and $I_L(t = 0) = I_{L0} = \frac{V_{BAT}}{R_L}$

Replacing V_{CL_LS} by $V_{CL\_HS} + V_{BAT}$ in *Equation 19*, *Equation 20* and *Equation 21* provides the expression of the energy dissipated in the high-side driver during the switch-off phase.

Table 6. E_{DEMAG1_HS} with $V_{BAT} < V_{CL\_LS} - V_{CL\_HS}$

Conditions	E_{DEMAG1_HS}: $V_{BAT} < V_{CL\_LS} - V_{CL\_HS}$
$R_L > 0\ \Omega$ with parallel resistor to the inductor	**Equation 22** $$(V_{CL\_HS} + V_{BAT})\left(\frac{\tau}{R_L}(V_{CL\_HS} + V_{BAT}) - \frac{\tau}{R_L // R_p}(V_{CL\_HS})\left(1 + \ln\left(\frac{R_p}{R_L + R_p} \cdot \frac{V_{CL\_HS} + V_{BAT}}{V_{CL\_HS}}\right)\right)\right)$$ with $\tau = \frac{L}{R_L}$, valid if $R_p > \frac{V_{CL\_HS}}{V_{BAT}} R_L$
$R_L > 0\ \Omega$ No parallel resistor to the inductor: $R_P = +\infty$	**Equation 23** $$\frac{L}{R_L}(V_{CL\_HS} + V_{BAT})\left(I_{L0} - \frac{V_{CL\_HS}}{R_L}\ln\left(\frac{V_{CL\_HS} + V_{BAT}}{V_{CL\_HS}}\right)\right)$$ with $I_{L0} = \frac{V_{BAT}}{R_L}$
$R_L = 0\ \Omega$ $R_P = +\infty$	**Equation 24** $$\frac{1}{2}LI_{L0}^2\left(\frac{V_{CL\_HS} + V_{BAT}}{V_{CL\_HS}}\right)$$ with $I_{L0} = \frac{V_{BAT}}{R_L}$

Figure 10. Equivalent circuit during the demagnetization of a high-side with parallel resistor, $V_{BAT} < V_{CL\_LS} - V_{CL\_HS}$

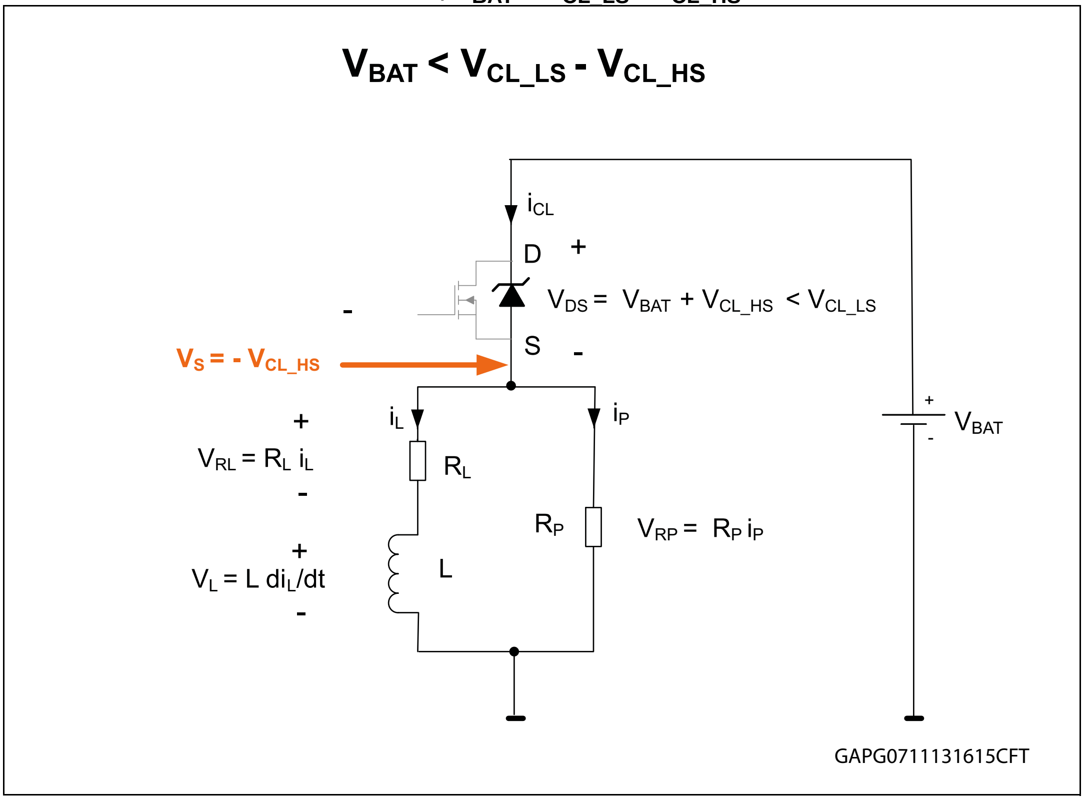

V_L is negative during the turn-off phase according to the used sign convention, since $di_L/dt < 0$.

3.3.2 Demagnetization energy with $V_{BAT} > V_{CL\_LS} – V_{CL\_HS}$

As discussed in the *Section 2.2.2*, the gate-drain clamp is activated.

From an electrical point of view *Figure 7* and *Figure 10* are equivalent, regardless whether the switch is in high-side or low-side configuration (provided that $V_{BAT} < V_{CL\_LS} – V_{CL\_HS}$).

Figure 11. Equivalent circuit during the demagnetization of a high-side with parallel resistor, $V_{BAT} > V_{CL\_LS} - V_{CL\_HS}$

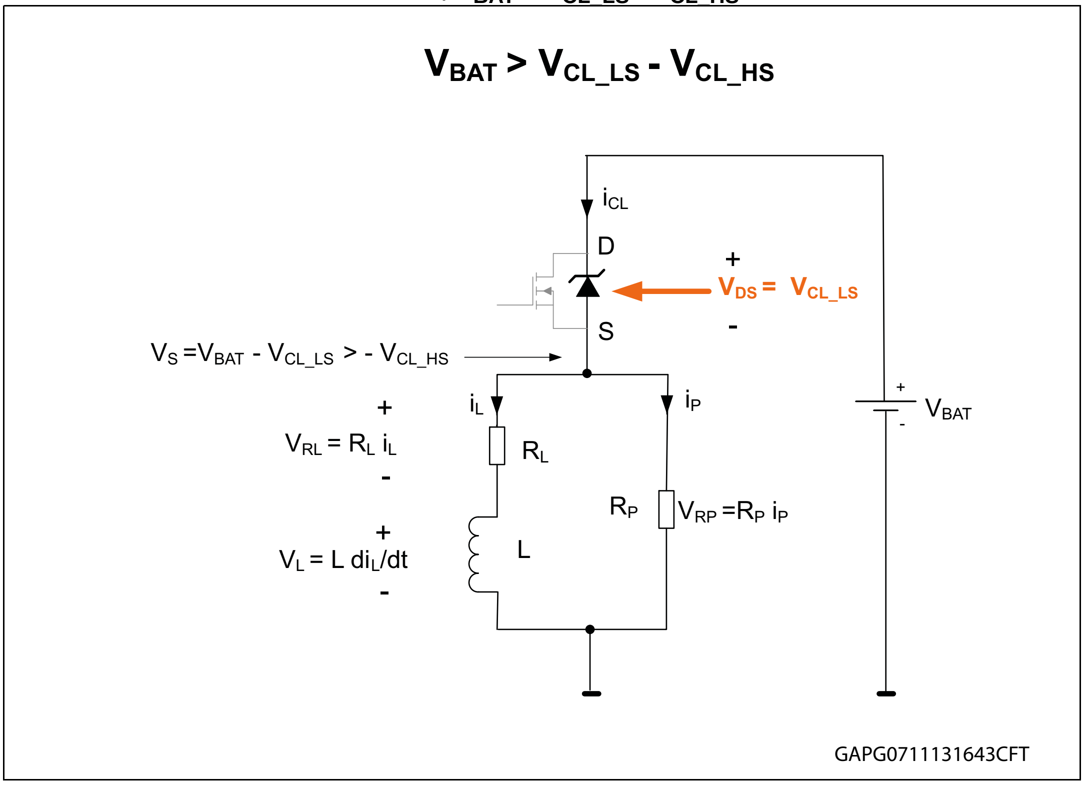

Therefore, the results for the low-side configured outputs are directly applicable to the high-side configured outputs when $V_{BAT} < V_{CL\_LS} - V_{CL\_HS}$.

Table 7. E_{DEMAG2_HS} with $V_{BAT} > V_{CL\_LS} - V_{CL\_HS}$

Conditions	E_{DEMAG2_HS}: $V_{BAT} > V_{CL\_LS} - V_{CL\_HS}$
$R_L > 0\ \Omega$ with parallel resistor to the inductor	**Equation 25** $$V_{CL\_LS}\left(\frac{\tau}{R_L}V_{CL\_LS} - \frac{\tau}{R_L // R_p}(V_{CL\_LS} - V_{BAT})\left(1 + \ln\left(\frac{R_p}{R_L + R_p}\cdot\frac{V_{CL\_LS}}{V_{CL\_LS} - V_{BAT}}\right)\right)\right)$$ with $\tau = \frac{L}{R_L}$, valid if $R_p > \frac{V_{CL\_LS} - V_{BAT}}{V_{BAT}} R_L$

Table 7. E_{DEMAG2_HS} with $V_{BAT} > V_{CL\_LS} - V_{CL\_HS}$ (continued)

Conditions	E_{DEMAG2_HS}: $V_{BAT} > V_{CL\_LS} - V_{CL\_HS}$
$R_L > 0\ \Omega$ No parallel resistor to the inductor: $R_P = +\infty$	**Equation 26** $$\frac{L}{R_L}V_{CL\_LS}\left(I_{L0} - \frac{V_{CL\_LS} - V_{BAT}}{R_L}\ln\left(\frac{V_{CL\_LS}}{V_{CL\_LS} - V_{BAT}}\right)\right)$$ with $I_{L0} = \frac{V_{BAT}}{R_L}$
$R_L = 0\ \Omega$ $R_P = +\infty$	**Equation 27** $$\frac{1}{2}LI_{L0}^2\left(\frac{V_{CL\_LS}}{V_{CL\_LS} - V_{BAT}}\right)$$ with $I_{L0} = \frac{V_{BAT}}{R_L}$

3.4 Clamping energy at high battery voltage

3.4.1 Qualitative analysis when the gate-drain clamp is active

The gate-drain clamp is activated

As we will see, the theoretical condition with $R_L = 0\Omega$ doesn't provide accurate results, especially when V_{BAT} is close or equal to V_{CL_LS}.
However, we can draw two qualitative observations from the simplified expression of E_{DEMAG} (*Equation 17*).

Equation 17:

$$\lim_{\substack{R_P \to +\infty \\ R_L \to 0}} E_{DEMAG\_LS} = \lim_{\substack{R_P \to +\infty \\ R_L \to 0}} E_{DEMAG2\_LS} = \frac{1}{2}LI_{L0}^2\left(\frac{V_{CL\_LS}}{V_{CL\_LS} - V_{BAT}}\right)$$

E_{DEMAG} is higher than the energy stored in the inductor

Since $V_{BAT} < V_{CL\_LS}$, we see from the simplified expression of E_{DEMAG}(*Equation 17*), that the dissipated energy in the output MOSFET is higher than the energy stored in the inductor ($\frac{1}{2}LI_{L0}^2$). This is due to the fact that the battery provides additional energy to the output MOSFET during the turn-off phase.

E_{DEMAG} increases faster than a square function of V_{BAT}

I_{L0} is proportional to the battery voltage ($I_{L0} = \frac{V_{BAT}}{R_L}$), and the term $\frac{1}{2}LI_{L0}^2$ is proportional to the square of I_{L0} and therefore to the square of V_{BAT}.

Moreover the factor

$$\frac{V_{CL\_LS}}{V_{CL\_LS} - V_{BAT}} = \frac{1}{1 - \frac{V_{CL\_LS}}{V_{BAT}}}$$

increases rapidly as V_{BAT} gets closer to the clamping voltage. The impact of this term is sometimes overlooked, although it is responsible for a drastic increase of the clamp energy at high V_{BAT}.

Assuming that the inductance is constant, independently from the current level I_{L0} (no saturation of the inductance), the demagnetization energy increases faster than a square function of V_{BAT}, especially when the battery voltage is close to the clamping voltage.

Figure 12. Contribution of the factor 1 / (1 - (V_{CL_LS}/V_{BAT})) to the increase E_{DEMAG} with V_{BAT}

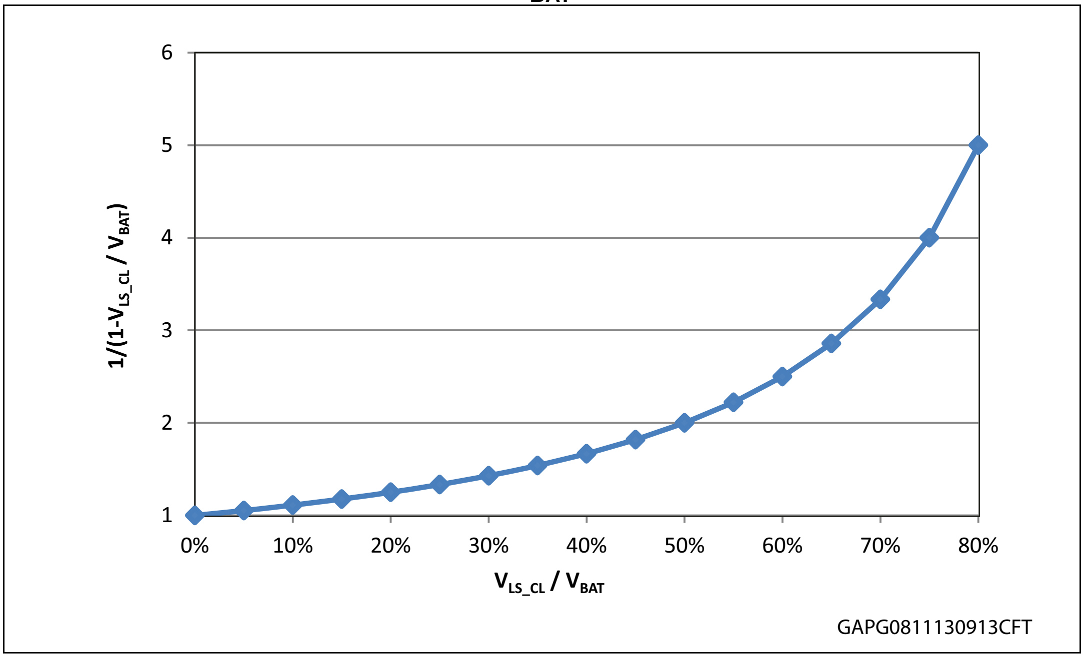

The gate-source clamp is activated

From *Equation 24*, we observe that the dissipated energy in a high-side configured output, when the gate-source clamp is activated exceeds the energy stored in the inductor. It is also due to the additional energy which is supplied by the battery during the turn-off phase.

Equation 24:

$$\lim_{\substack{R_P \to +\infty \\ R_L \to 0}} E_{DEMAG1\_HS} = \frac{1}{2} L I_{L0}^2 \left(\frac{V_{CL\_HS} + V_{BAT}}{V_{CL\_HS}} \right)$$

Moreover, the demagnetization energy in this case increases faster than a square function of V_{BAT} due to the additional term: $1 + \frac{V_{BAT}}{V_{CL\_HS}}$.

3.4.2 Example of a low-side configured output of the L99MC6

Table 8. Low-side output - conditions

Parameter	Value
L	512 mH
R_L	46 Ω
R_P	400 Ω
V_{CL_LS}	35 V (typical value of the L99MC6)

Figure 13 shows that under the considered conditions (*Table 8*), the simplification $R_L = 0\ \Omega$ leads to a significant overestimation of the dissipated energy in the low-side driver. The overestimation is even greater as V_{BAT} increases (*Table 9*).

Table 9. Overestimation of E_{DEMAG} caused by the simplification: $R_L = 0\ \Omega$

V_{BAT}	E_{DEMAG} [mJ] $R_L > 0\Omega$, $R_P = 400\Omega$	E_{DEMAG} [mJ] $R_L = 0\Omega$ (w/o R_P)	Overestimation of E_{DEMAG} [mJ] with $R_L = 0\ \Omega$
6V	0.9	5.2	4.3
10V	6.6	17	11.4
16V	26.9	57.1	30.2
24V	83.6	221	137

Figure 13. E_{DEMAG_LS} vs V_{BAT} – Example of a low-side output of the L99MC6

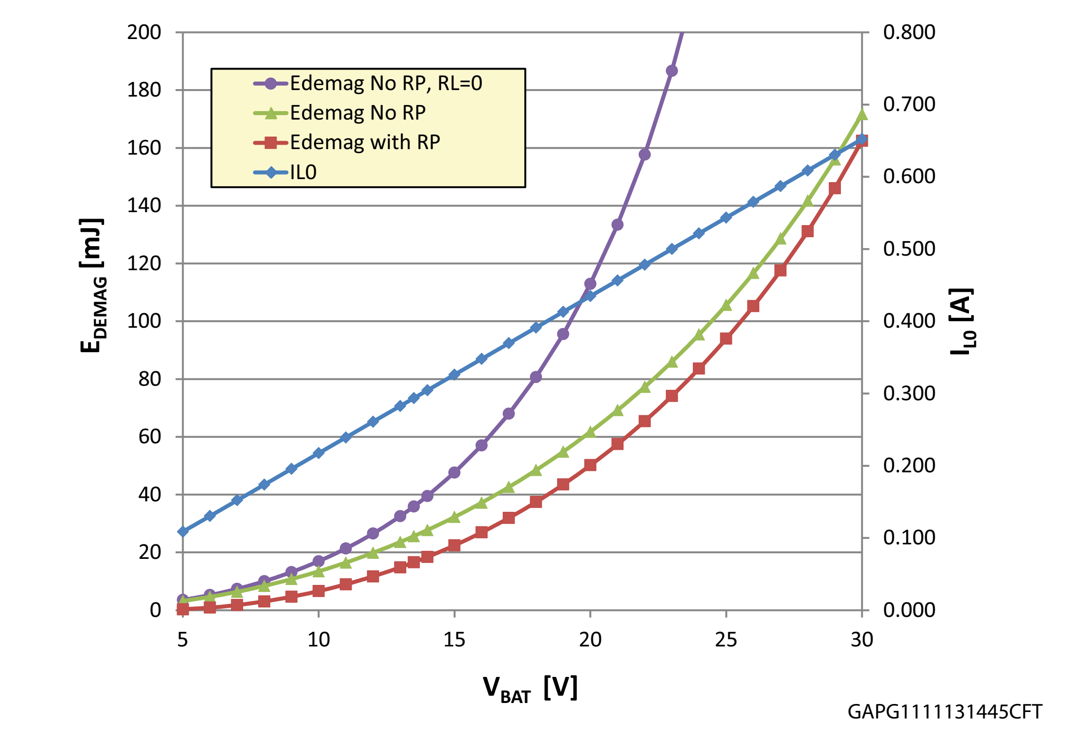

Figure 14 displays the relative evolution of E_{DEMAG} with V_{BAT}. The reference is for

V_{BAT} = 13 V and R_P is not considered.
We observe that the E_{DEMAG_LS} increases faster than a square function of V_{BAT}, as previously anticipated. For example, doubling V_{BAT} from 13 V to 26 V increases E_{DEMAG_LS} by a factor 5.
A slight additional increase of V_{BAT} to 28.6 V (2.2 x 13 V) increases E_{DEMAG_LS} by a factor 6.35.

Figure 14. Example - Relative E_{DEMAG_LS} to $E_{DEMAG@VBAT=13V}$ versus V_{BAT}/13V (No parallel resistor)

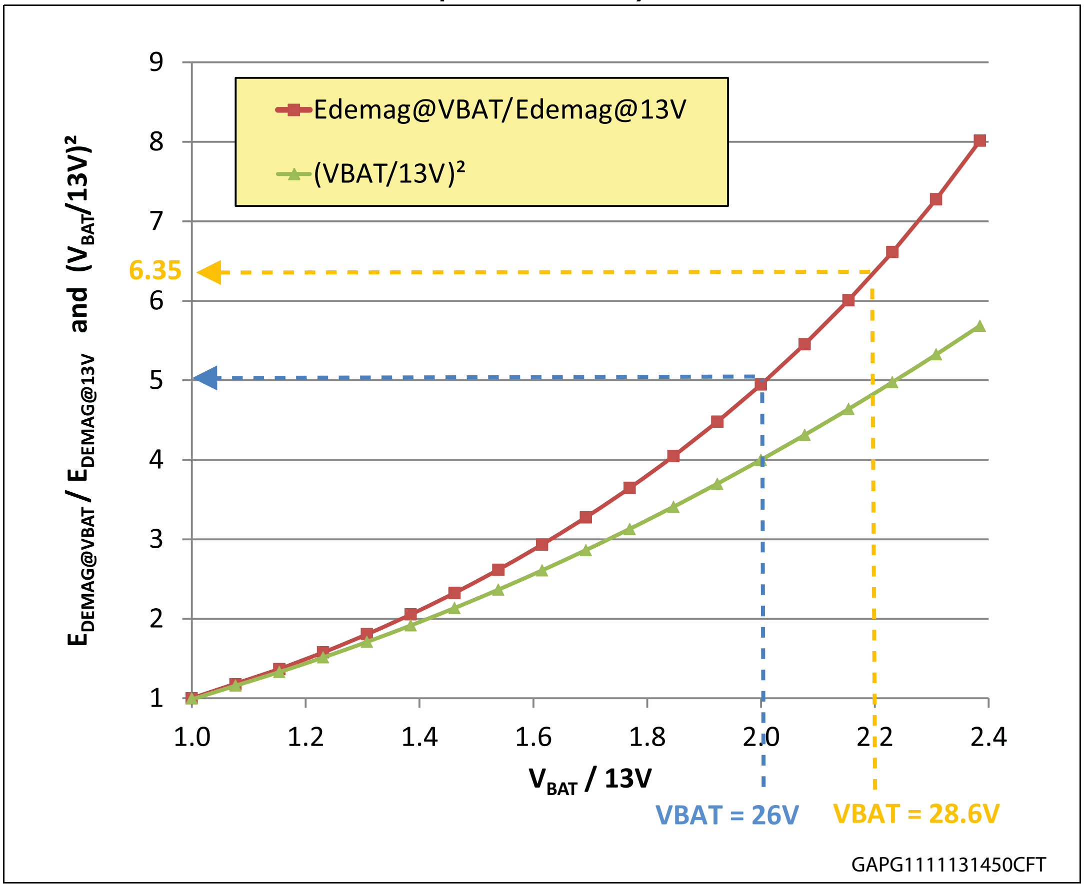

3.4.3 Example of a high-side configured output of the L99MC6

Table 10. high-side output - conditions

Parameter	Value
L	512mH
R_L	46Ω
R_P	400Ω
V_{CL_HS}	16V (typical value of the L99MC6)
V_{CL_LS}	35V (typical value of the L99MC6)

Figure 15 shows that under the considered conditions, the simplification $R_L = 0\ \Omega$ leads to a significant overestimation of the dissipated energy in the high-side driver. The overestimation is even greater as V_{BAT} increases.

Table 11. Energy values vs battery voltages

VBAT	E_{DEMAG} [mJ] R_L>0Ω , R_P = 400Ω	E_{DEMAG} [mJ] R_L=0Ω (w/o R_P)	Overestimation of E_{DEMAG} [mJ] with R_L=0Ω
6V	1.9	5.7	3.8
10V	8.2	18.5	10.3
16V	29.9	57.1	30.2
24V	83.6	221	137

Considering that the demagnetization energy is the same for a low-side driver and for a high-side driver of the L99MC6 for $V_{BAT} \geq 16V$, the conclusions for high battery voltages are also applicable.

Figure 15. E_{DEMAG_HS} vs V_{BAT} – Example of a high-side output of the L99MC6

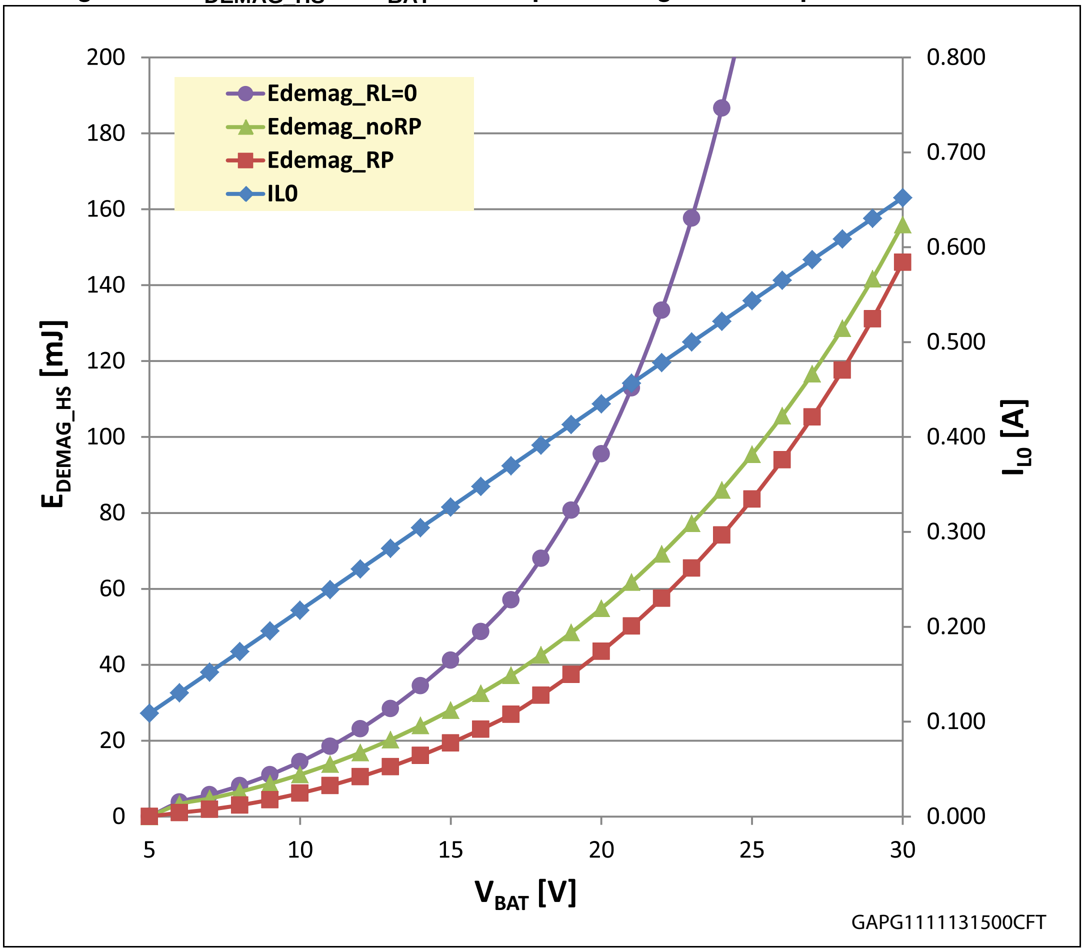

3.4.4 Conclusions

From this example, we see that calculating E_{DEMAG} with $R_L = 0\ \Omega$ can lead to a huge overestimation of the dissipated energy in the low-side and high-side drivers, especially at high V_{BAT}. Therefore, it is more accurate to take into account the impact of load resistance R_L (and the parallel resistor $R_{P,}$ if any) on the demagnetization energy.

E_{DEMAG} increases with V_{BAT} at a faster rate than the quadratic function of V_{BAT}. Therefore, the developer must be careful about the device compatibility to the considered load, if the outputs drive inductive loads at high battery voltages.

4 Energy capability and load compatibility

Although the avalanche condition is prevented by the active clamp, the inductive energy capability of the L99MC6 and L9733 is limited. As the MOSFET operates in linear mode with a high V_{DS}, a high power is dissipated during the turn-off phase. The sudden increase of the junction temperature causes a stress to the device. The maximum device capability must not be exceeded in order to avoid permanent damages.

This aspect must be taken into account during the development phase.

It is possible to identify two main mechanisms that can lead to the device failure:

- The temperature during the demagnetization rises quickly (depending on the inductance) and the uneven energy distribution on the power surface can cause the presence of a hot spot causing the device failure with a **single pulse**.
- Like in normal operation, the lifetime of the device is affected by the fast thermal variation as described by the Coffin-Manson law. A **repetitive** demagnetization energy causing a temperature variation above 60K will cause a shorter life time.

These considerations lead to two simple design rules:

- The energy dissipated in the application conditions during the corresponding demagnetization time must be lower than the device capability for the same t_{DEMAG}.
- In case of a repetitive pulse, the average temperature variation of the device should not exceed 60K at turn-off.

To fulfill these rules, the designer must calculate the energy dissipated in the output mosfet at turn-off and the corresponding t_{DEMAG} and then compare it with the device capability as shown in the example *Section 4.2*.

4.1 Guideline

Step1: Calculation of t_{DEMAG} and E_{DEMAG}

This step consists in calculating the demagnetization time and energy dissipated in the output under the defined load and application conditions. The relevant formulas are collected in *Table 16* and *Table 17*.

Step2: Maximum energy capability of the device at the relevant t_{DEMAG}

The designer must determine the device output capability in terms of demagnetization energy from the datasheet relevant curve with the same demagnetization time.

Note that the curve providing the current capability for inductive loads of the L99MC6 is valid for the specific conditions: V_{BAT} = 13.5V and R_L = 0 Ω (*Figure 16*).

The L99MC6 provides data under the following conditions:

- Single pulse, with T_{JSTART} = 150°C: it is applicable for switch-off conditions, which occur rarely
- Repetitive pulse with T_{JSTART}=125°C: it is applicable for switch-off conditions, with a high occurrence rate. It is applicable with time between two occurrences is long enough to allow the junction temperature to decrease to 125°C
- Repetitive pulse with T_{JSTART}=100°C: it is applicable for switch-off conditions, with a high occurrence rate. It is applicable if the time between two occurrences is long enough to allow the junction temperature to decrease to 100°C

Even if E_{DEMAG} dissipated in the application conditions is below the maximal energy allowed by the device with the same inductance (at R_L = 0 Ω and R_L = 13.5 V), it does not automatically mean that the load compatibility is given. Indeed, it is possible that a lower E_{DEMAG} in the application conditions is dissipated in a shorter time (t_{DEMAG}), resulting in a higher power dissipation and therefore a higher junction temperature increase.

The developer must verify that the energy which has been calculated in the step1 is below the maximum energy capability of the device with the corresponding demagnetization time.

Step3: Confirmation by measurements

It is recommended to perform bench tests in the real application conditions.

This phase is key because it allows verifying that the load data (inductance and resistance), which are used for the calculations in step1 and step2, are representative of the real application. It avoids either an underdimensioning of the system and therefore unexpected failures, or overdimensioning with the involved extra-costs for external protection devices.

Some sources of mismatch between calculations and measurement can be:

- A mismatch between the calculation R_L and the real R_L. Indeed, R_L is in general specified only at room temperature. Since the winding is made of copper, its resistance is subject to variations due to temperature.
- measuring the inductance with a LCR meter by applying a small AC signal does not take into account the impact of the DC voltage bias of the inductance in the real application
- the decrease of the inductance at high currents (saturation of the inductor) might not be taken into account
- self-heating effects of the load on R_L and L are not considered

4.2 Example of L99MC6 driving a relay with a low-side driver

Table 12. Application conditions

Parameter	Value
Type of output	Configurable output (OUT1,2 or 3), configured as low-side switch
L	512 mH
R_L	46 Ω
R_P	400 Ω
V_{CL_LS}	35V (typical value of the L99MC6)

Table 12. Application conditions (continued)

Parameter	Value
$V_{BAT,MAX}$ (jump start)	24V → I_{L0} @$V_{BAT,MAX}$ = 0.522A, low probability of occurrence
$V_{BAT,TYP}$	13.5V → I_{L0} @$V_{BAT,TYP}$ = 0.293A, nominal conditions

Step 1: Calculation of t_{DEMAG} and E_{DEMAG}

The demagnetization energy and the demagnetization time under the conditions listed in *Table 12* are given by *Equation 19* and *Equation 11*:

E_{DEMAG_LS} = 83.6 mJ and t_{DEMAG_LS} = 11.7 ms with $V_{BAT,MAX}$ = 24 V

E_{DEMAG_LS} = 16.6 mJ and t_{DEMAG_LS} = 4.2 ms with $V_{BAT,TYP}$ = 13.5 V

The validity condition of *Equation 19* is satisfied since $R_P > 21\ \Omega$ (for V_{BAT} = 24 V) and $R_P > 74\ \Omega$ (for V_{BAT} = 13.5 V).

Step 2: Maximum energy capability of the L99MC6 at the relevant t_{DEMAG}

Considering the type of output, the relevant diagram of the datasheet is: "Configurable switch LSD – Maximum turn-off current versus inductance" (*Figure 16*).

Note: *If the considered output is one of the fixed low-side switches (outputs 4, 5, 6) or one of the outputs configured as high-side driver, the relevant diagrams are respectively "Fixed LSD switch – Maximum turn-off current versus inductance" and "Configurable switch HSD–Maximum turn-off current versus inductance".*

Figure 16. Datasheet L99MC6 - Inductive energy capability of configurable channels, configured as low-side switch

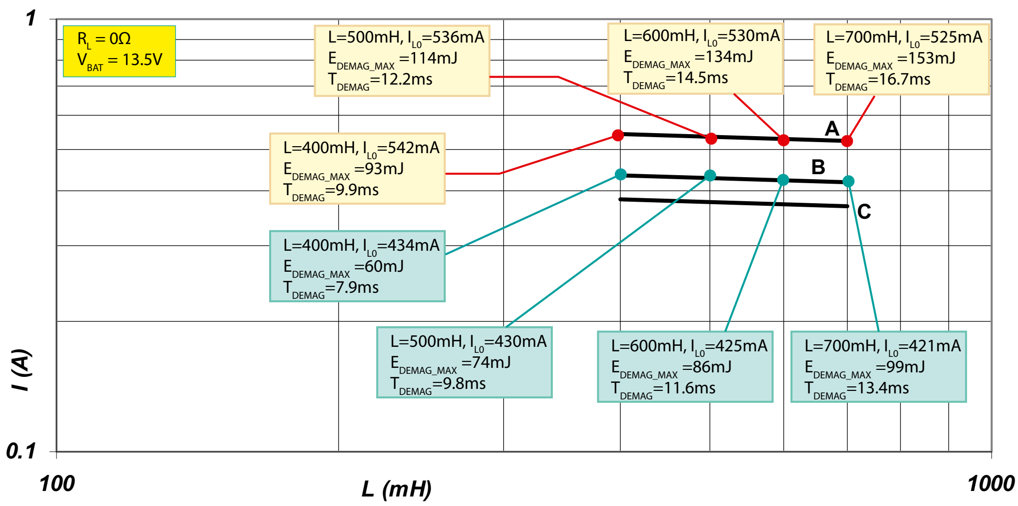

A: Single pulse, T_j = 150 °C

B: Repetitive pulse, T_j = 100 °C

C: Repetitive pulse, T_j = 125 °C

GAPG1111131528CFT

Figure 16 displays the maximum allowed current of outputs 1, 2 or 3 (configurable outputs) in low-side configuration, driving an inductive load. Different conditions (single or repetitive pulses) and start temperature (junction temperature right before the switch-off phase of the MOSFET) are considered. The test conditions for these curves are V_{BAT} = 13.5 V and R_L = 0 Ω. These conditions are different from the application conditions and are therefore not directly applicable to our specific case.

One way to verify the load compatibility consists in building the curve $E_{DEMAG,MAX}$ versus the corresponding t_{DEMAG} from the relevant I-L plot of *Figure 16*, where $E_{DEMAG,MAX}$ is the maximum energy which the device can sustain.

Condition 1: The jump start conditions ($V_{BAT,MAX}$ = 24 V) have a very low probability of occurrence. The single pulse is applicable. From *Figure 17*, we see that the energy capability of the device for a single pulse at 11.7ms is higher than the energy dissipated in the application conditions.

Table 13. E_{DEMAG_MAX} and corresponding t_{DEMAG} for a single pulse, T_{JSTART} = 150°C, R_L = 0 Ω, V_{BAT} = 13.5 V

L [mH]	I_{L0} [A]	t_{DEMAG} [ms] R_L = 0 Ω V_{BAT} = 13.5 V	E_{DEMAG_MAX} [mJ] R_L = 0 Ω V_{BAT} = 13.5 V
400	0.542	9.9	93
500	0.536	12.2	114
600	0.530	14.4	134
700	0.525	16.7	153

Figure 17. E_{DEMAG_MAX} vs t_{DEMAG} for a single pulse T_{JSTART} = 150°C

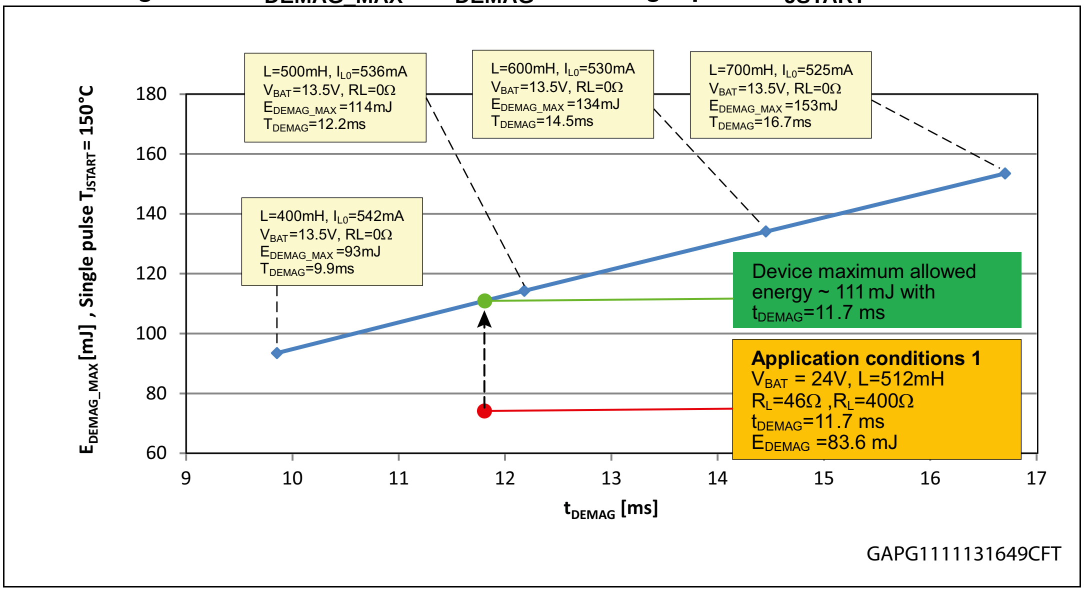

Condition 2 ($V_{BAT,TYP}$ = 13.5 V) corresponds to the nominal conditions with T_J = 100 °C: The repetitive pulse condition is applicable. Building the curve $E_{DEMAG,MAX}$ versus the corresponding t_{DEMAG} for repetitive pulses at T_{JSTART} = 100 °C from *Figure 16*, we obtain *Table 14* and *Figure 18*.

Table 14. E_{DEMAG_MAX} and corresponding t_{DEMAG} for a repetitive pulse with T_{JSTART} = 100 °C, R_L = 0 Ω, V_{BAT} = 13.5 V

L [mH]	I_{L0} [A]	T_{DEMAG} [ms] R_L=0Ω V_{BAT}=13.5V	E_{DEMAG_MAX} [mJ] R_L=0Ω V_{BAT}=13.5V
400	0.434	7.9	60
500	0.430	9.8	74
600	0.425	11.6	86
700	0.421	13.4	99

Figure 18. E_{DEMAG_MAX} vs t_{DEMAG} for repetitive pulse T_{JSTART} = 100°C

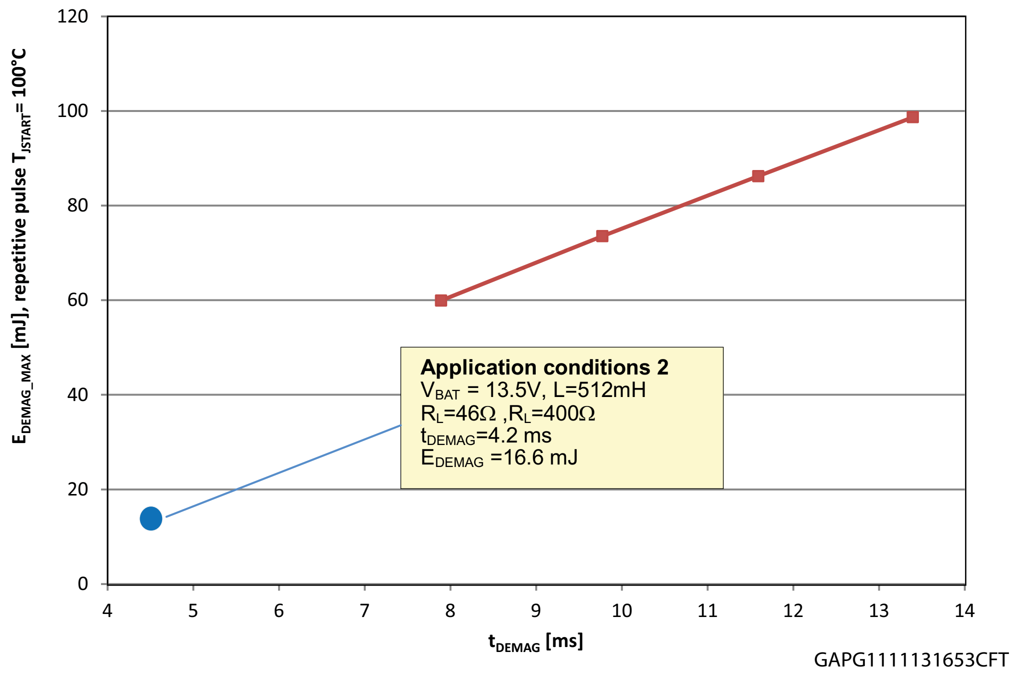

However, the data provided by the datasheet for repetitive pulse conditions at T_{JSTART} = 100 °C have demagnetization times which are longer than 4.2 ms (calculated in step1).

Another possibility to calculate E_{DEMAG_MAX} for a given t_{DEMAG} consists in using the empiric property: $\frac{E_{DEMAG\_MAX}}{\sqrt{t_{DEMAG}}}$ is constant.

For example, using the first row of *Table 14*, we have:

$$E_{DEMAG\_MAX2} = E_{DEMAG\_MAX1}\sqrt{\frac{t_{DEMAG2}}{t_{DEMAG1}}} = 60 \cdot \sqrt{\frac{4.2}{7.9}} = 43.7\text{mJ}$$

Since the energies calculated in the step 1 are below the device maximum capability for the same demagnetization time, the low-side output of the L99MC6 is compatible with the load and the switch-off conditions previously defined.

Appendix A Documents reference

1. Configurable 6-channel device (L99MC6, DocID16523)
2. Octal self configuring low/high side driver (L9733, DocID11319)
3. VIPower M0-5 and M0-5Enhanced high-side drivers (UM1556, DocID023520)
4. Transistor protection by Transil™ (AN587, DocID3599)

Appendix B Glossary

Table 15. Glossary

Abbreviation	Description
V_{BAT}	Battery voltage
V_{DS}	MOSFET drain-source voltage
V_S	MOSFET source voltage
V_{ZENER_LS}	Zener voltage of the gate-drain clamp
V_{ZENER_HS}	Zener voltage of the gate-source clamp
V_{CL_LS}	Clamping voltage when the gate-drain clamp is active
V_{CL_HS}	Clamping voltage when the gate-source clamp is active Sign convention : $V_{CL\_HS} > 0$
V_F	Typical diode forward voltage
V_{GS_TH}	MOSFET gate-source threshold voltage
L	Inductance
V_L	Voltage across the inductor
R_L	Inductor DC resistance
V_{RL}	Voltage across R_L
R_P	Resistor in parallel to the inductive load
V_{RP}	Voltage across R_P
i_P	Current through R_P
i_L	Current through the inductor
I_{L0}	Inductor current right before the turn-off phase: $I_{L0} = I_L(t=0)$
E_{DEMAG_LS}	Demagnetization energy of a low-side: dissipated energy in the low-side
E_{DEMAG1_HS}	Demagnetization energy of a high-side when $V_{BAT} \leq V_{CL\_LS} - V_{CL\_HS}$
E_{DEMAG2_HS}	Demagnetization energy of a high-side when $V_{BAT} \geq V_{CL\_LS} - V_{CL\_HS}$
t_{DEMAG_LS}	Demagnetization time of a low-side
t_{DEMAG1_HS}	Demagnetization time of a high-side when $V_{BAT} \leq V_{CL\_LS} - V_{CL\_HS}$
t_{DEMAG2_HS}	Demagnetization time of a high-side when $V_{BAT} \geq V_{CL\_LS} - V_{CL\_HS}$

Appendix C Summary of the demagnetization energy

Table 16. Demagnetization time and demagnetization energy for a low-side configured output

Load conditions	t_{DEMAG_LS} Demagnetization time	E_{DEMAG_LS} Demagnetization energy in the low-side configured output
With parallel resistor to the inductor $R_L > 0\Omega$	$\frac{L}{R_L}\ln\left(\frac{V_{CL\_LS}}{V_{CL\_LS}-V_{BAT}}\frac{R_L // R_p}{R_L}\right)$	$V_{CL\_LS}\left(\frac{\tau}{R_L}V_{CL\_LS}-\frac{\tau}{R_L // R_p}(V_{CL\_LS}-V_{BAT})\right)\left(1+\ln\left(\frac{R_p}{R_L+R_p}\cdot\frac{V_{CL\_LS}}{V_{CL\_LS}-V_{BAT}}\right)\right)$ with $\tau = \frac{L}{R_L}$, valid if $R_p > \frac{V_{CL\_LS}-V_{BAT}}{V_{BAT}} R_L$
Without parallel resistor to the inductor $R_L > 0\Omega$	$\frac{L}{R_L}\ln\left(\frac{V_{CL\_LS}}{V_{CL\_LS}-V_{BAT}}\right)$	$\frac{L}{R_L}V_{CL\_LS}\left(I_{L0}-\frac{V_{CL\_LS}-V_{BAT}}{R_L}\ln\left(\frac{V_{CL\_LS}}{V_{CL\_LS}-V_{BAT}}\right)\right)$ with $I_{L0} = \frac{V_{BAT}}{R_L}$
Without parallel resistor to the inductor $R_L = 0\Omega$	$\frac{LI_{L0}}{V_{CL\_LS}-V_{BAT}}$	$\frac{1}{2}LI_{L0}^2\left(\frac{V_{CL\_LS}}{V_{CL\_LS}-V_{BAT}}\right)$ with $I_{L0} = \frac{V_{BAT}}{R_L}$

Table 17. Demagnetization time and demagnetization energy for a high-side configured output

V_{BAT} range	Load conditions	t_{DEMAG_HS} Demagnetization time	E_{DEMAG_HS} Demagnetization energy in the high-side configured output
$V_{BAT} \le V_{CL\_LS} - V_{CL\_HS}$	With parallel resistor to the inductor $R_L > 0\Omega$	$\frac{L}{R_L}\ln\left(\frac{V_{CL\_HS}+V_{BAT}}{V_{CL\_HS}}\frac{R_L // R_p}{R_L}\right)$ with $R_L//R_p = \frac{R_pR_L}{R_p+R_L}$	$(V_{CL\_HS}+V_{BAT})\left(\frac{\tau}{R_L}(V_{CL\_HS}+V_{BAT}) - \frac{\tau}{R_L // R_p}(V_{CL\_HS})\left(1+\ln\left(\frac{R_p}{R_L+R_p}\cdot\frac{V_{CL\_HS}+V_{BAT}}{V_{CL\_HS}}\right)\right)\right)$ with $\tau = \frac{L}{R_L}$, valid if $R_p > \frac{V_{CL\_HS}}{V_{BAT}}R_L$
	Without parallel resistor to the inductor $R_L > 0\Omega$	$\frac{L}{R_L}\ln\left(\frac{V_{CL\_HS}+V_{BAT}}{V_{CL\_HS}}\right)$	$\frac{L}{R_L}(V_{CL\_HS}+V_{BAT})\left(I_{L0} - \frac{V_{CL\_HS}}{R_L}\ln\left(\frac{V_{CL\_HS}+V_{BAT}}{V_{CL\_HS}}\right)\right)$ with $I_{L0} = \frac{V_{BAT}}{R_L}$
	Without parallel resistor to the inductor $R_L = 0\Omega$	$\frac{LI_{L0}}{V_{CL\_HS}}$	$\frac{1}{2}LI_{L0}^2\left(\frac{V_{CL\_HS}+V_{BAT}}{V_{CL\_HS}}\right)$ with $I_{L0} = \frac{V_{BAT}}{R_L}$

Table 17. Demagnetization time and demagnetization energy for a high-side configured output (continued)

V_{BAT} range	Load conditions	t_{DEMAG_HS} Demagnetization time	E_{DEMAG_HS} Demagnetization energy in the high-side configured output
$V_{BAT} \geq V_{CL\_LS} - V_{CL\_HS}$	With parallel resistor to the inductor $R_L > 0\Omega$	$\frac{L}{R_L}\ln\left(\frac{V_{CL\_LS}}{V_{CL\_LS}-V_{BAT}}\frac{R_L//R_p}{R_L}\right)$ with $R_L//R_p = \frac{R_pR_L}{R_p+R_L}$	$V_{CL\_LS}\left(\frac{\tau}{R_L}V_{CL\_LS}-\frac{\tau}{R_L//R_p}(V_{CL\_LS}-V_{BAT})\left(1+\ln\left(\frac{R_p}{R_L+R_p}\cdot\frac{V_{CL\_LS}}{V_{CL\_LS}-V_{BAT}}\right)\right)\right)$ with $\tau = \frac{L}{R_L}$, valid if $R_p > \frac{V_{CL\_LS}-V_{BAT}}{V_{BAT}}R_L$
	Without parallel resistor to the inductor $R_L > 0\Omega$	$\frac{L}{R_L}\ln\left(\frac{V_{CL\_LS}}{V_{CL\_LS}-V_{BAT}}\right)$	$\frac{L}{R_L}V_{CL\_LS}\left(I_{L0}-\frac{V_{CL\_LS}-V_{BAT}}{R_L}\ln\left(\frac{V_{CL\_LS}}{V_{CL\_LS}-V_{BAT}}\right)\right)$ with $I_{L0} = \frac{V_{BAT}}{R_L}$
	Without parallel resistor to the inductor $R_L = 0\Omega$	$\frac{LI_{L0}}{V_{CL\_LS}-V_{BAT}}$	$\frac{1}{2}LI_{L0}^2\left(\frac{V_{CL\_LS}}{V_{CL\_LS}-V_{BAT}}\right)$ with $I_{L0} = \frac{V_{BAT}}{R_L}$

Revision history

Table 18. Document revision history

Date	Revision	Changes
22-Nov-2013	1	Initial release.